International Journal of Biology Research
www.biologyjournal.in
ISSN: 2455-6548
Received: 19-04-2026, Accepted: 20-05-2026, Published: 04-06-2026
Volume 11, Issue 2, 2026, Page No. 71-81

Synthesis, characterization, antimicrobial and photocatalytic activity of cobalt oxide nanoparticles

Dr B B Waykar, Dhanashree A Kirdat*
Department of Zoology, Dr Babasaheb Ambedkar Marathwada University, Chhatrapati Sambhajinagar, Maharashtra, India
Corresponding Author: Dhanashree A Kirdat
DOI: https://doi.org/10.66856/ijbr.2026.11.2.11031

Abstract
At present work cobalt oxide nanoparticle (Co_3O_4 NPs) were synthesized via simple coprecipitation method using KOH and NH_4OH as the reducing agents. The synthesised materials were applied for the removal of methylene blue (cationic) and Phenol Red (anionic) dyes from the water. Comparative study was done to test the efficacy of the synthesized nanomaterials for the dye degradation, antibacterial and antifungal activities. Further the synthesised material was characterised with X-ray diffraction (XRD) analysis, Fourier Transform Infra Spectroscopy (FTIR), Field Emission Scanning Electron Microscopy (FESEM), Raman spectroscopy and UV-vis spectroscopy to check the purity, crystalline size, and shape of the formed NPs. The Co_3O_4 NPs synthesised using KOH as the reducing agent showed noteworthy antimicrobial properties as compared to that of NH_4OH as the reducing agent and sunlight induced photocatalytic activity for environmental remediation.

Keywords: Cobalt oxide nanoparticles, antibacterial, antifungal activity, environmental remediation, photocatalytic activity

Introduction

The scientific field of nanotechnology is concerned with the analysis of materials at the nanoscale, which is typically defined as 1 to 100 nm [1]. The enhanced surface-to-volume ratio and quantum confinement effects in these size ranges enable nano-sized materials to exhibit new characteristic optical, electrical, and magnetic properties compared to their bulk counterparts [2]. Owing to these novel properties, nanoparticles are capable of being employed in various technological, environmental, energy, and biological domains, including lithium-ion batteries, solar cells, hydrogen storage, and magnetic data storage [3]. Many nanoparticles comprising of metallic, magnetic, fluorescent (quantum dot), polymeric, and protein-based nanoparticles, are employed in the biomedical applications [4]. Because the size and shape of magnetic metal oxide nanoparticles can be altered, they have drawn particular attention. The material used to make the nanoparticles can have a direct effect on their magnetic, electrical, and chemical properties [5]. Synthetic dyes, particularly in the textile industry, have genotoxic and carcinogenic properties. India's rivers are being contaminated by textile dye effluents due to high chemical oxygen demand and organic matter concentrations. Dyes can alter water pH and temperature due to increasing suspended particles, like chlorides, nitrates, and other metals. They also increase BOD and COD levels, impacting water quality, aquatic creatures' behaviour, and survival [6][7].These pollutants reduce dissolved oxygen content, posing a threat to aquatic life and humans [8].

Water contamination is a top concern, causing diseases like cholera, typhoid, and cancer. The World Health Organisation estimates 2.3 million people die annually due to water pollution. About 100,000 dyes are used annually, negatively impacting ecosystems [6]. Research aims to reduce environmental impact by removing or degrading dye from wastewater using various biological and physicochemical strategies [9].The effective photocatalyst ought to have a large surface area to adsorb additional contaminants (dyes), a high photon capture rate to generate electron-hole pairs and a high electron carrier recombination suppression rate [10, 11]. Nanoparticles-based reductive degradation offers advantages such as ease of use, high catalytic efficacy, speed, affordability, and industrial application, making it simple to use [12].

Though a lot has been accomplished, the identification of any nanomaterial for visible light photocatalysis along with high antimicrobial activity remains elusive. Cobalt oxide (Co_3O_4) nanoparticles are worthy candidates owing to their mixed oxidation states of Co^{2+} and Co^{3+}, which facilitate charge transfer dynamics in such a way that photocatalytic activity is enhanced. Also, the unique cubic spinel structure ensures better chemical stability and reactivity. Recent studies indicate that Co_3O_4 has a much higher antimicrobial action compared to conventional metal oxides, which may be due to its ability to produce reactive oxygen species (ROS) because of better penetration into the outer membranes of bacterial cells, causing injury or rupture to their cell wall.

Considerable attention has been paid to the most stable phase of Co_3O_4, which has a direct bandgap of 1.48–2.19 eV and is employed as a p-type semiconductor. The hydrothermal process, which is less expensive and regarded as a green synthesis, often involves the reduction and precipitation of chemical agents in order to create Co_3O_4 NPs [13]. One of the five distinct oxidation states of cobalt oxide, which is a transition metal oxide, is Co, CoO_2, Co_2O_3, CoO (OH), CoO_2, and Co_3O_4 [14]. In addition, Co_3O_4 has a characteristic cubic spinel structure with Co_2^+ ions filling the tetrahedral sites (8a) and Co_3^+ ions occupying the octahedral sites (16d). It also displays mixed oxidation states such as Co_2^+ and Co_3^+.Thus it is highly stable and simple to synthesise in an open environment and have been extensively developed for applications in nano-magnets, photo-catalysts, electro-catalysts, magnetic sensors, semiconductors, imaging devices, supercapacitors, batteries, and coating materials [15, 16]. Among many varieties, Co_3O_4

NPs have unique qualities that make them suitable for electro-catalysis, gas sensing, and for lithium storage. Co_3O_4 NPs have been also applied to radiation therapy, immunisation, and cancer diagnosis. Moreover, it functions well as a cofactor of vitamin B_{12} and is useful in the detection of methanol, glucose, and amino acids [17]. Co_3O_4 nanoparticles undergo photocatalytic degradation, converting organic chemicals into smaller, safer molecules through light energy, involving dye conversion and chromophoric group dissolution.

Methylene blue (MB) also called as Methylthioninium chloride is a positively charged organic dye that is widely used to colour a variety of materials, including leather, office supplies, paper, and clothing [6]. Water polluted by MB content is generated in the textile, plastic, and dye industries [18]. MB is one of the dyes that is recognised to be harmful to the aquatic life [19]. Even at low concentrations, dye in industrial wastewater can physically block sunlight from reaching the water, reducing photosynthesis and placing stringent limits on the amount of organic matter that can be present in contaminated water. Long-term exposure to MB can also be harmful to human health, as it can cause renal damage, central nervous system malfunction, and gastrointestinal problems [6].

Phenol Red (PR), also referred to as Phenolsulfonphthalein, is a poisonous substance that is commonly employed as a pH indicator in cell biology laboratories to assess kidney function. It irritates skin and eyes when it comes into touch with them, also it is bad for the digestive and respiratory systems when inhaled [20]. PR is also very harmful and hazardous for animals and plants living in water because it has carcinogenic and mutagenic effects [21].

According to a World Health Organisation research report in almost 50% of cases, the bacteria *E.coli* and *Staphylococcus aureus* have demonstrated resistance to certain conventional antibiotics. Scientists have been searching for antibiotics to combat germs since the 20th century. However, the antibiotic resistance has increased due to genetic exchanges and chromosomal alterations. *Staphylococcus aureus* and *E. coli* cause prevalent illnesses, with over 50% of cases showing resistance to certain antibiotics [22]. Cobalt oxide nanoparticles synthesised by using cobalt nitrate hexhydrate as a precursor exibits antibacterial activity against the pathogens *S. aureus* and *E. coli* [23]. Co_3O_4 NPs are harmless in the body at lower levels [24].

The present work is focused on the synthesis of Co_3O_4 nanomaterials by facile co-precipitation method and studying antimicrobial and photocatalytic activity on dyes.

Materials and Methods

1. Materials Used

Cobalt (II) Nitrate AR (Hexahydrate) [$CO_3O_4.6H_2O$], KOH and NH_4OH, Methylene Blue, [$C_{16}H_{18}CIN_3.S_xH_2O$], Phenol Red GR [$C_{19}H_{14}O_6S$], KOH (AR Grades Purity> 99.00%) were purchased as the initiating materials and used without any further purifications.

2. Preparation of CO_3O_4 Nanoparticles

For the preparation of Co_3O_4 nanoparticles, $Co(NO_3)_2.6H_2O$ was added into 100 ml of deionized water to form 0.1M of solution and stirred for 60 minutes to form the precursor solution. 3M-KOH was prepared separately in 200 ml. deionized water and was added dropwise into the precursor solution under constant stirring until pH reached 10. The final solution was subjected to post stirring for 60 minutes and allowed to age overnight. The obtained gel was washed three times with deionized water and ethanol to remove if any kind of impurities were present followed by drying at room temperature to obtain CO_3O_4 nanoparticles. For improving crystalline ordering, the synthesised CO_3O_4 nanoparticles were annealed in a muffle furnace at 300°C for 3 hours.

To prepare 3M-NH_4OH solution 40.81 ml of liquid ammonia solution (NH_3) was diluted in 59.19 ml of distilled water to make up the volume up to 100 ml. This reducing agent solution was then added drop wise in the precursor solution until pH reached 10. The final solution was subjected to post stirring for 60 minutes and allowed to age overnight. The obtained gel was washed three times using deionized water and ethanol to remove if any kind of impurities were present followed by drying at room temperature to obtain CO_3O_4 nanoparticles. For improving crystalline ordering, the synthesised CO_3O_4 nanoparticles were annealed in a muffle furnace at 300°C for 3 hours.

KOH-synthesised cobalt oxide nanoparticles demonstrated enhanced antibacterial and antifungal activities, photocatalytic dye degradation, and distinct platelet structures with smaller particle size and larger surface area as compared to the agglomerated NPs [25, 26].

3. Characterization

After the successful synthesis of Co_3O_4 NPs, various techniques were used to characterize the nanoparticles. X-ray diffraction (XRD) was used to examine the synthesised nanoparticle's crystalline structure. XRD patterns were recorded in the 20–70° 2θ range. Based on the width at half maxima, crystallite sizes were estimated using the Debye-Scherrer equation. Using FTIR analysis technique, the functional groups present in the samples were confirmed within the range of 4000–200 cm^{-1}. Using energy-dispersive X-ray spectroscopy in conjunction with scanning electron microscopy, the surface morphology and shape of the Co_3O_4 NPs were verified (SEM-EDX).The Raman spectra were recorded using Explora Plus spectrometer with diode pumped solid state laser at 532 nm. UV-Vis spectroscopy was employed using PerkinElmer UV-Vis Lambda 25 spectrophotometer to study the optical properties of the oxide nanoparticles.

4. Antibacterial Activity

The antibacterial activity of Cobalt Oxide nanoparticles was tested by using Disk diffusion method against *S.aureus and P.aeruginosa*. All glasswares were sterilized in autoclave at 121ºC prior to experimental work. Nutrient agar media was used for this experiment.1mg/ml of Cobalt oxide nanoparticle solution were prepared in DMSO. A sterile disc loaded with test solution with size 6 mm (10 µl) were inserted in nutrient agar plates having different bacterial culture. The plates were kept in incubator at 37ºC for 24 hours. After 24 hours the clear zone around disk which corresponds to bacterial growth inhibition was measured using Vernier caliper in millimeters unit.

5. Antifungal Activity

The antifungal activity of Co_3O_4 NPs was examined against pathogenic fungi *Aspergillus niger* (MZ435863) and *Aspergillus fumigatus* (MZ435922) using diffusion method.

The potato dextrose agar (PDA) was used as culture media and prepared in accordance with the previous report. 50 µg/ml concentration Co_3O_4 NPs solution was prepared in dimethyl sulphoxide (DMSO). Later, Co_3O_4 NPs solution was added to PDA media and mixed well in petri plates and then media is allowed to solidify. The mycelia of fungi were inoculated in the centre of each petri plate and then incubated at a temperature of 29 ±1°C under suitable conditions. The pure PDA media without Co_3O_4 NPs solution were used as a control. The percentage fungal growth inhibition was using the following formula:

$$\text{Inhibition}=\frac{\text{Growth zone of control-Growth zone of treatment}}{\text{Growth zone of control}}\times 100$$

6. Photo-Catalytic Activity Procedure

The PCA (photo-catalytic activity) of the synthesised cobalt oxide NPs was evaluated by degrading Methylene Blue (MB) and Phenol Red dyes (PR). 10 ppm solutions of the dyes were prepared respectively. 0.2 gm/litre of the synthesized catalysts 3M-KOH and 3M-NH_4OH were added to 100 ml of the prepared solutions and exposed to the sunlight. The suspension was kept in dark for around 30 minutes before its exposure to the sunlight in order to ensure adsorption-desorption equilibrium. After regular intervals of 10 mins. 3 ml of the samples were extracted and analysed for dye residual concentration by UV-vis spectrophotometer (Perkin Elmer) at the characteristic absorbance of the dye. Beer-Lambert's law was used to estimate the degradation percentages of the dyes with time as follows:

$$\%\,\text{Degradation}=\frac{c_0-c_t}{c_t}\times 100=\frac{A_0-A_t}{A_t}\times 100$$

Here, the initial and concentration at time t of the respective dye are represented by C_0 and C_t respectively, while the respective absorbance's were represented by A_0 and A_t respectively. Rate constant (k) of the nano catalysts were calculated by assuming pseudo-first order kinetics using following equation:

$$\text{Rate constant, } k=\frac{1}{t}\ln\left[\frac{c_0}{c_t}\right]$$

Results and Discussion

1. FTIR Analysis

FTIR technique was used to determine the nature of bonds and functional groups size that were present in the synthesised nanomaterials at room temperature absorption peaks. The FTIR transmittance spectrum of Co_3O_4 nanoparticles (Fig.1.) was recorded at room temperature, within the frequency range of 500–4000 cm^{-1} [27]. The characteristic peaks of Co_3O_4 nanoparticles were seen at 557.68 cm^{-1} and 658.52 cm^{-1} for 3M-KOH nanoparticles and 555.63 cm^{-1} and 658.52 cm^{-1} for 3M-NH_4OH respectively. These peaks confirmed the spinel structure of the synthesized nanoparticles [28, 29]. Absence of any other peaks indicates high purity of the nanomaterials.

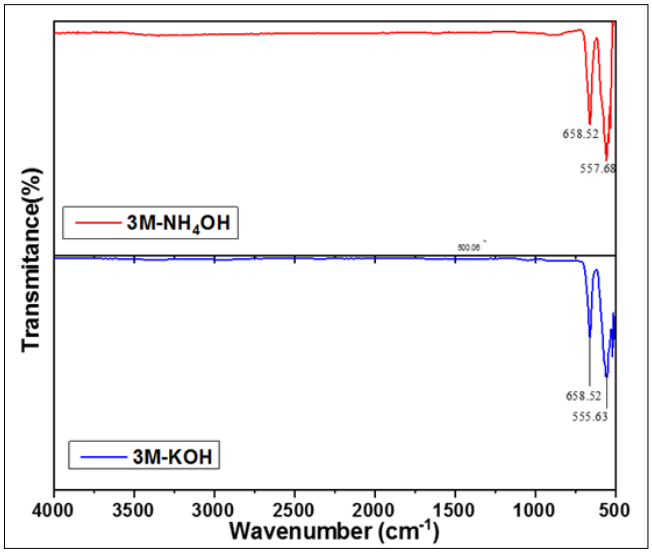

Fig 1: Representative FTIR images of NH_4OH and KOH

The peak detected at 658.52 cm^{-1} for both 3M-KOH and 3M- NH_4OH used synthesized Co_3O_4 nanoparticles was attributed to the metal-oxide bond stretching vibrations of Co – O in Co_3O_4. The bridging vibration of the Co_3^{+}– O bond in an octahedral site is characterised by this peak [11, 30, 27].We can therefore verify the sample's purity based on the data above.

2. Raman Analysis

The Raman spectrum(Fig.2.) of the Co_3O_4 nanoparticles in the range of 532 nm shows six obvious peaks located at 461 nm, 504 nm, 591nm, 669 nm, 1962 nm, 3121 nm using 3M-KOH and 464 nm, 504 nm, 591 nm, 669 nm, 1962 nm, 3121 nm using 3M-NH_4OH as the reducing agents [31][15][32]. These major bands can be attributed to the carbonyl functional groups, amides, and Co3O4 NPs, respectively [6].

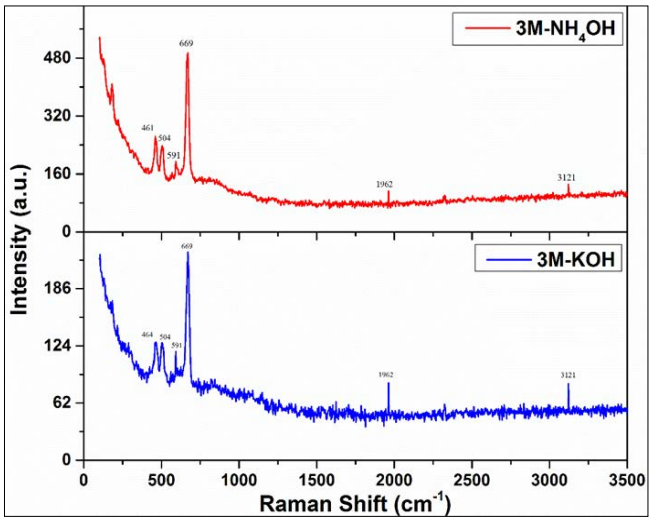

Fig 2: Representative Raman images of NH_4OH and KOH

The band at 461 cm^{-1} could potentially originate from surface imperfections resulting from the oxidation of Co on the surface of Co_3O_4 [33].The bands at 461 and 504 cm^{-1} belong to skeletal bending vibrations of C-N-C [34].The results thus indicated the successful formation of cobalt oxide nanoparticles.

3. X-ray Diffraction Analysis

The structural characterization of Cobalt oxide nanoparticles (Co_3O_4 NPs) has been done by using XRD pattern (Fig.3.) recorded by Bruker D8 Advanced Diffractometer with 0.15405 nm Cu-Kα radiation source. The obtained XRD patterns confirmed the crystalline nature, single phase and purity of synthesized Co_3O_4 NPs as represented in Fig. 3 for Co_3O_4 NPs-KOH and Co_3O_4 NPs-NH_4OH. The diffraction peaks corresponding to hkl values (111), (220), (311), (222), (400), (422), (511),(440) and (533) planes confirms the cubic crystal structure and Fd3m space group of synthesized Co_3O_4 NPs and well matched with the standard data JCPDS card no 073-1701 [35, 38].The high quality of Co_3O_4 NPs can be seen as no additional peak of any particular impurity was present [1, 39].

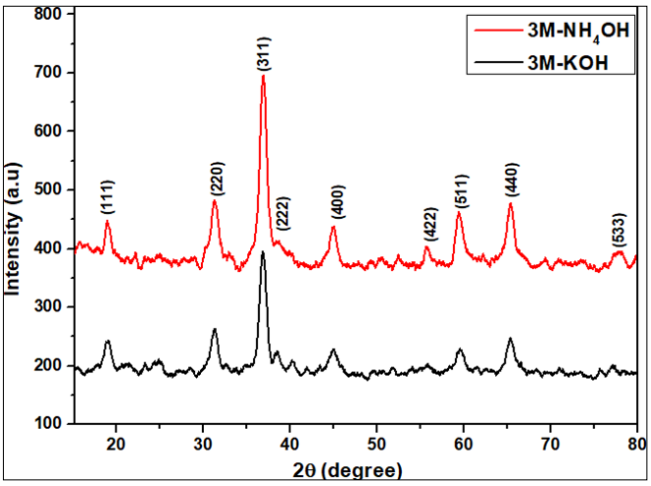

Fig 3: Representative XRD patterns of 3M-NH_4OH and 3M-KOH

The crystalline sizes (D) of Co_3O_4 NPs were calculated by using the Scherrer formula for the sharpest peaks corresponding to (220), (311) and (440) planes as follows by equation (4) [2]:

$$D = \frac{k\lambda}{\beta\cos\theta}$$

Where, k is called shape factor (k =0.9), λ=0.15405 nm is the wavelength Cu-K_α radiation source of the incident radiation, and β represents the Full Width at Half Maximum (FWHM) of diffraction peaks. The calculated average crystallite sizes for Co_3O_4 NPs-KOH and was found to be 6.7 nm [40, 41]. Hence the obtained data confirms the nanocrystalline nature of synthesized Co_3O_4 NPs found to be 6.7 nm. Hence the obtained data confirms the nanocrystalline nature of prepared materials for the NPs prepared in 3M-KOH.

4. UV Analysis

Fig. 4. Shows the UV–Vis optical absorbance spectra of Co_3O_4 nanoparticles in the 190 nm to 600 nm. The characteristic absorption peak corresponding the 3M-KOH and 3M-NH_4OH Co_3O_4 nanoparticles were found at around 262 nm [42, 43]. Further, corresponding Tauc plots were plotted to calculate the optical band gaps of the nanoparticles. The Tauc equation used to estimate the direct band gap is given below:

$$(\alpha h\nu)^2 = A(Eg - h\nu)$$

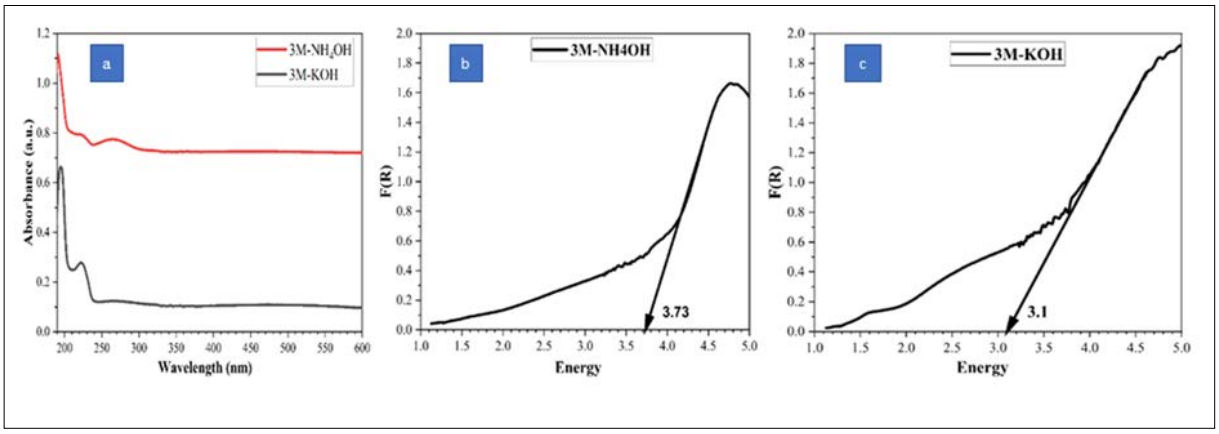

Fig 4: Representative of (a) UV–Visible spectrum of cobalt (III) oxide nanoparticles (b) NH_4OH and (c) KOH energy bands

Here hν is the photon energy, A is the constant determined by the type of transition, α is the absorption coefficient and E_g is the optical band gap. The optical band gap E_g was calculated by extrapolating the linear portion of the graph onto the *hν* axis [38].As calculated from the Tauc plot, the optical band gaps of 3M-KOH and 3M- NH_4OH Co_3O_4 nanoparticles were found to be 3.1 and 3.73 eV respectively. The smaller band gap of the 3M-KOH [35].

5. Field Emission Scanning Electron microscopy (FESEM) Analysis

The high-resolution Field Emission Scanning Electron microscopy (FESEM) Technique was used to study the surface morphology of synthesized Co_3O_4 NPs. (Fig.5) represents the FESEM images along with particle size distribution profile of Co_3O_4 NPs-KOH and Co_3O_4 NPs-NH_4OH. The synthesized materials were shaped into spherical and mixed shapes through nucleation, growth, and aggregation [35]. Images revealed less agglomerated synthesised particles of Co_3O_4 NPs-KOH as compared to Co_3O_4 NPs-NH_4OH [13]. The particle morphology in case of Co_3O_4 NPs-KOH was found to be platelet like structure with good regularity in the shape.

The highly agglomerated nanoparticles were observed in case of Co_3O_4 NPs-NH_4OH [16, 12].

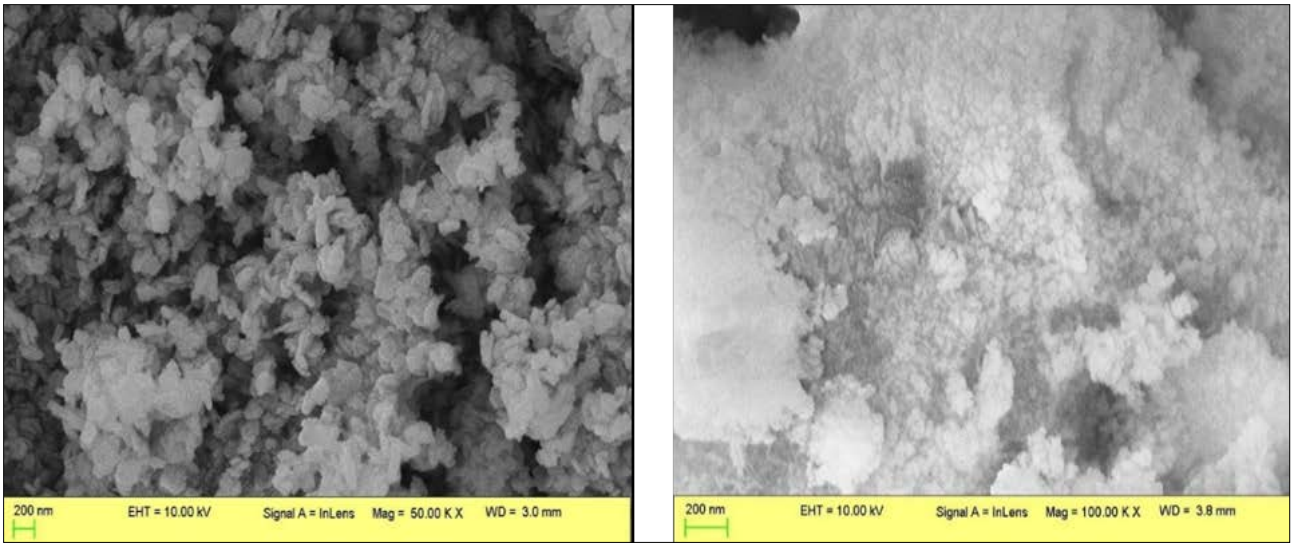

Fig 5: Representative FESEM images for a) Co_3O_4 NPs-KOH b) Co_3O_4 NPs-NH_4OH

For Co_3O_4 NPs synthesized using 3M-KOH, the average particle sizes measured using image -J software were 98.12 nm, while for Co_3O_4 NPs-NH_4OH, significant agglomeration was detected, making the particle size calculation challenging [15, 25]. Therefore, Co_3O_4 NPs synthesized using 3M-KOH exhibited greater photocatalytic and antimicrobial activities than Co_3O_4 NPs synthesized using 3M-NH_4OH due to regularity in particle shape, size and reduced agglomeration.

6. EDX Analysis

The Co_3O_4 nanoparticles synthesised had a nanostructure composed of metal and oxygen stabilization/interface. The presence of Co and O elements was validated by EDX spectroscopy ((Fig.5.). Co_3O_4 nanoparticle phase is clarified by their Co and O existence, and no other element is evolved during the processes in both the synthesis using KOH and NH_4OH respectively [35].

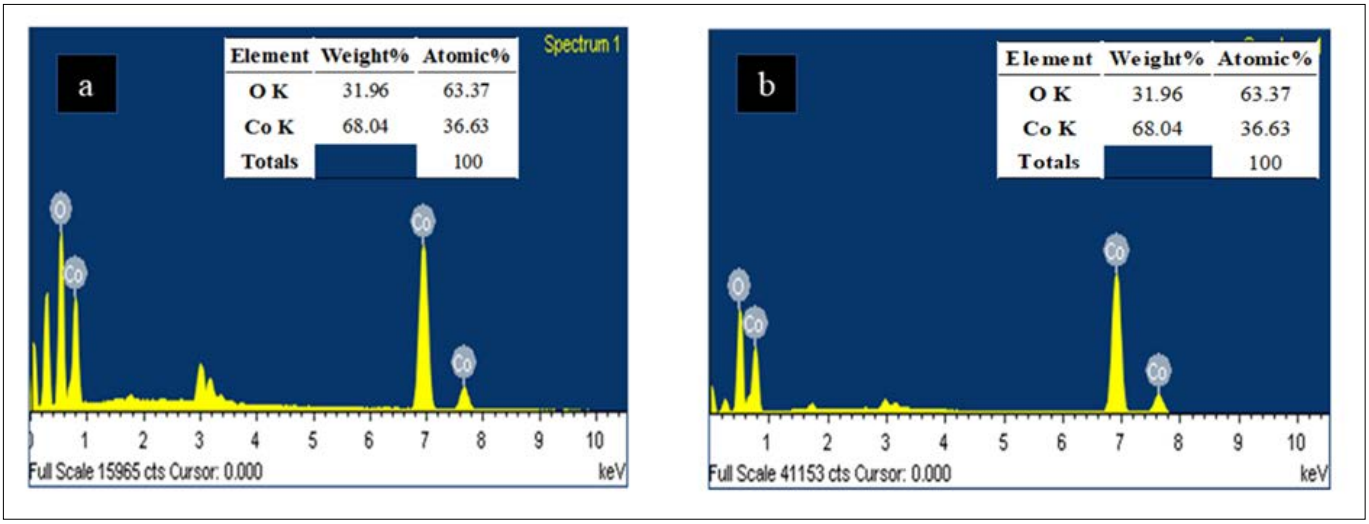

Fig 6: a) EDX spectra of Co_3O_4 nanoparticles synthesised by using 3M-KOH; b) EDX spectra of Co_3O_4 nanoparticles synthesised by using 3M- NH_4OH

7. Antibacterial Activity

The synthesised Co_3O_4 nanoparticles' antibacterial efficacy against strains of both gram-positive and gram-negative bacteria was investigated using the disc diffusion method. To investigate the effect of nanoparticle concentration on antibacterial activity, Co_3O_4 nanoparticles that were generated chemically and biologically at concentrations of 0.05 mg/ml were tested against strains of *S.aureus*, *P.aerugenosa*, bacteria. The antibacterial activity of Co_3O_4 nanoparticles was compared to that of the positive control, ciprofloxacin Co_3O_4 nanoparticles [44]. The reduced bacterial growth observed in this investigation for both Co_3O_4-NPs against *S. aureus* [24], *P. aeruginosa* [45], is shown in Table 1.

Table 1: Antibacterial activity as indicated by growth-inhibition zone of different concentration of Co_3O_4 NPs against different strains of bacteria.

Sr. No.	Sample Code	*Staphylococcus aureus*	*Psedomonas Aeruginosa*
1	3M-KOH	7.18	10.72
2	3M-NH_4OH	1.02	9.93

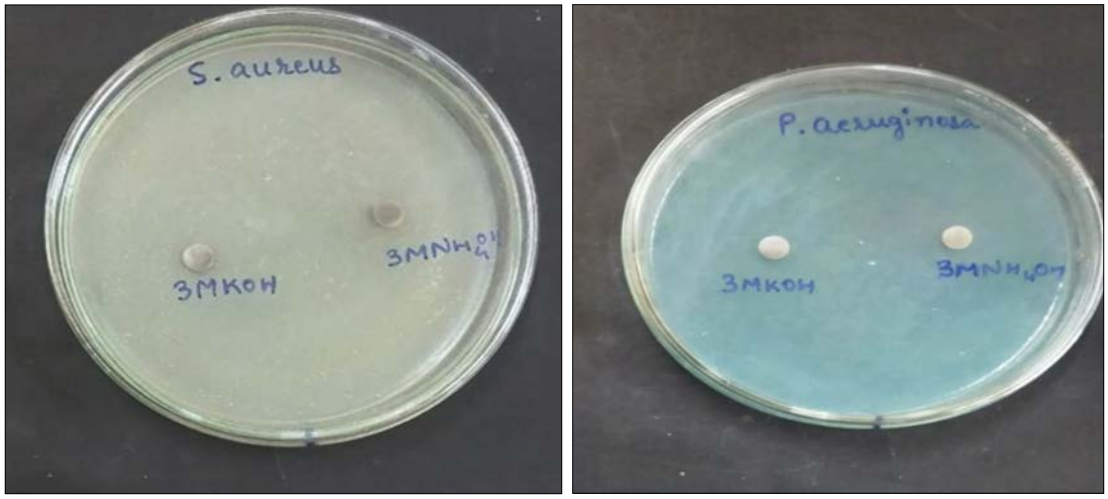

Fig 7: Zone of inhibition for (a) *S.Aureus* and (b) P.Aeruginosa shown by Co_3O_4 NPs synthesised with KOH and NH_4OH

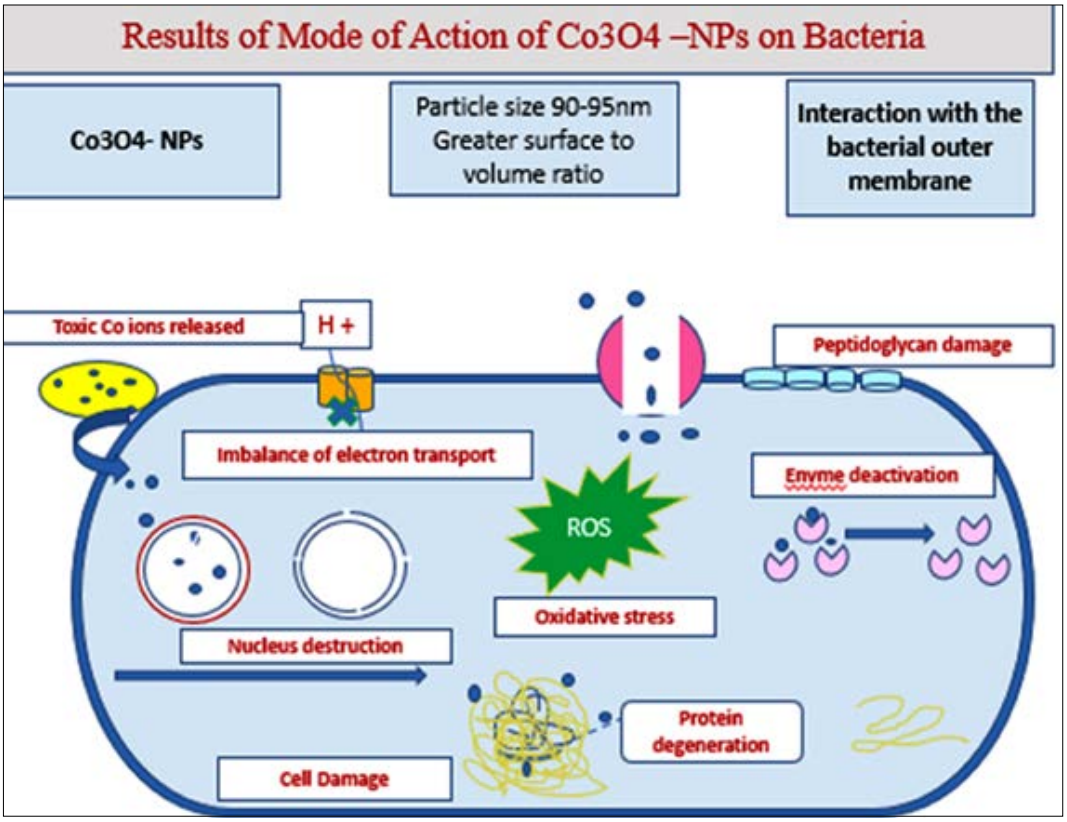

Fig 8: Mechanism of action of nanoparticles in bacterial cells.

According to the results, as shown in Fig.7 (a) and (b) both Co_3O_4 NPs synthesised with KOH and NH_4OH had better antibacterial qualities. The reason for this could be the higher surface area to volume ratio of the NPs, which could interact with the outer bacterial cell membrane through electrostatic interaction. Metal ions, with their 98.12 nm thickness, can easily penetrate bacterial strains peptidoglycan-covered cell walls, rupturing the wall and allowing Co_3O_4 nanoparticles to enter. This leads to the production of ROS and suppresses the production of nucleus and DNA, ultimately resulting in cell death [30, 37].

8. Antifungal Activity

The Fig.9 and 10 (a) and (b) respectively represents the results of antifungal activity of Co_3O_4 NPs. It can be seen that in control plates

The selected fungi grown entirely with 90 mm growth zone. The inhibited growth of fungi was observed when treated with Co_3O_4 NPs which suggest the potential fungicidal nature of nanomaterial. Table 2 shows the growth zone (mm) and percentage of growth inhibition against *Aspergillus Niger* and *Aspergillus fumigatus*. In the case of *Aspergillus Niger* quiet similar activity was observed for both Co_3O_4 NPs. The excellent result was obtained in the case of 3M-KOH against *Aspergillus fumigatus* by attaining 80.25% growth inhibition. In contrast, no significant growth suppression was observed using 3M-NH_4OH against same fungus. The better performance of 3M-KOH can be attributed to the small particle size and uniform platelet like morphology. The current finding suggests that Co_3O_4 NPs can serve as an effective antifungal agent against *aspergillus* species.

Table 2: Antibacterial activity as indicated by growth-inhibition zone of different concentration of Co_3O_4 NPs against different strains of fungi.

Fungi	Growth zone (mm)			Percentage growth inhibition	
	Control	3M-KOH	3M-NH_4OH	3M-KOH	3M-NH_4OH
Aspergillus niger	90	29.454	28.498	67.27	68.33
Aspergillus fumigatus	90	17.772	90	80.25	-

Fig 9: Antifungal effect on the growth of *A.niger* treated with Co_3O_4 NPs synthesised with (a) KOH (b) NH_4OH

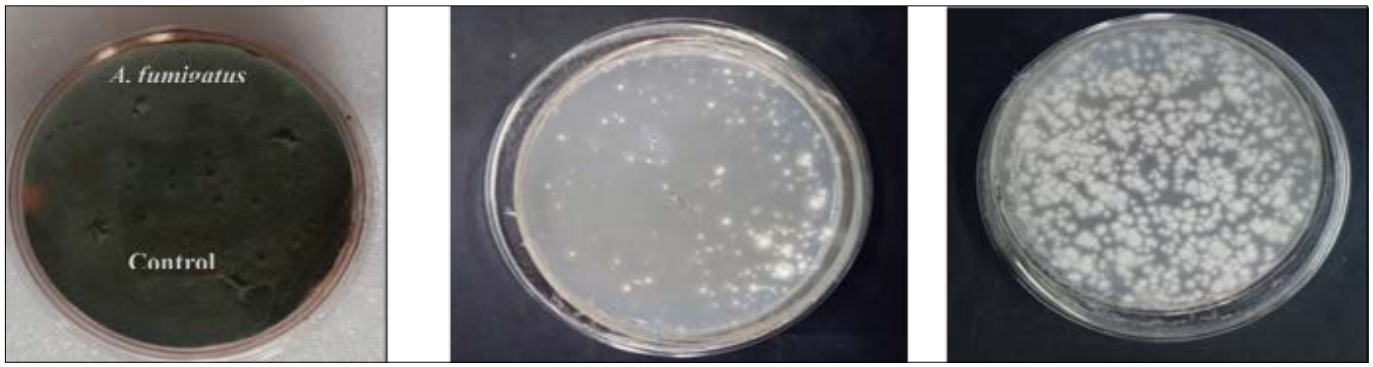

Fig 10: Antifungal effect on the growth of *A fumigatus* treated with Co_3O_4 NPs synthesised with (a) KOH (b) NH_4OH

It can be seen that in control plates the selected fungi grown entirely with 90 mm growth zone. The inhibited growth of fungi was observed when treated with Co_3O_4 NPs which suggest the potential fungicidal nature of nanomaterial. Table 2 shows the growth zone (mm) and percentage of growth inhibition against *Aspergillus Niger* and *Aspergillus fumigatus*. In the case of *Aspergillus Niger* quite similar activity was observed for both Co_3O_4 NPs. The excellent result was obtained in the case of 3M-KOH against *Aspergillus fumigatus* by attaining 80.25% growth inhibition as shown in Fig.10 (a) and (b). In contrast, no significant growth suppression was observed using 3M-NH_4OH against same fungus. The better performance of 3M-KOH can be attributed to the small particle size and uniform platelet like morphology. The current finding suggests that Co_3O_4 NPs can serve as an effective antifungal agent against aspergillus species.

Photocatalytic Degradation

In this study, the synthesized Co_3O_4 were used in the photodegradation of the dyes Phenol Red (PR) and Methylene Blue (MB) under sunlight to test their photocatalytic efficiency Fig.11 and 12 shows the UV-vis analysis of the degradation observed for the dyes PR and MB. As seen from the data, Co_3O_4 nanoparticles show low to moderate photocatalytic activity. Using 3M-NH_4OH catalyst, 18.80% of the PR was observed to be degraded, while using 3M-KOH, 58.29% of the dye was degraded [46]. This huge difference could be attributed to the structural, morphological and optical properties. Significant amount of agglomeration found in case of 3M-NH_4OH (via FESEM) could be one of the reasons of its lower photoactivity due to lower surface area to volume ratio. Another or an additional reason of this lower optical response to sunlight could be due to relatively higher band gap of the 3M-NH_4OH with respect to 3M-KOH.

Table 3: Details of the dye degradation of phenol red and methylene blue by synthesized Co_3O_4 nanoparticles using 3M-NH_4OH and 3M-KOH as reducing agent.

Catalyst Used	Phenol Red			Methylene Blue		
	% Degradation (120 Min)	K (Rate Constant)	Half Life (min)	% Degradation (120 Min)	K (Rate Constant)	Half Life (min)
3M-NH_4OH	18.80	0.00161	415.07	14.35	0.00144	481.35
3M-KOH	58.29	0.00741	93.54	15.89	0.00147	471.53

In contrast to this, both the catalyst showed poor photocatalytic activity against the methylene blue dye. This dye degraded 14.35% with the assistance of 3M-NH_4OH, while slightly better degradation of 15.89% was seen with 3M-KOH. This can be explained by the highly persistent nature of the methylene blue dye. The linear rate constants observed were mere 0.00144 and 0.00147 min^{-1} (Table 3), showing half-life in the range of 470-485 minutes. Among the two synthesized catalysts, 3M-KOH performed better in the degradation experiments. This may be due to the lower optical band gap and relatively better crystallinity than the 3M-NH_4OH Co_3O_4 nanoparticles.

The photocatalytic degradation experimental results indicate that KOH-synthesized Co_3O_4 achieved better dye degradation activity than NH_4OH-synthesized Co_3O_4. This performance is a result of various structural, morphological, and optical reasons that prompt changes in photocatalytic activity for the material.

Other unique factors contributing to the enhanced performance of KOH-synthesized Co_3O_4 include surface area and agglomeration. Analysis via FESEM revealed that KOH-synthesized Co_3O_4 possessed essentially a platelet morphological structure with more homogeneous nanoparticle dispersions, while the NH_4OH-synthesized Co_3O_4 agglomerated more severely. Because photocatalysis takes place primarily on the surface of the nanoparticles, a high surface area increases adsorption of dye molecules on the surface and enhances the interaction between the catalyst and the reactants, resulting in a more efficient degradation process.

Moreover, KOH-synthesized Co_3O_4 gave a higher crystalline character, with sharp diffraction peaks observed compared to NH_4OH-synthesized Co_3O_4, as indicated by XRD studies. The degree of crystallinity is critical in the case of photocatalysis as structural defects in nanomaterials act as charge recombination centers and hinder the overall charge carrier separation effectiveness. The broader peaks for NH_4OH-synthesized Co_3O_4 indicate smaller crystallites and structural defects which were probably responsible for fast recombination of photogenerated electron-hole pairs and hence lower photocatalytic activity.

An additional important factor is that the KOH-synthesized Co_3O_4 has a smaller optical band gap. UV-Vis spectroscopy revealed that the KOH-synthesized Co_3O_4 had a band gap of ~3.1 eV versus 3.73 eV for NH_4OH-synthesized Co_3O_4. Small band gaps provided for greater light absorption and electron excitation from the valence band to the conduction band. The enhancement of light absorption is directly responsible for the higher generation of electron-hole pairs that in turn can initiate the photocatalytic reactions to produce reactive oxygen species (ROS) including hydroxyl radicals (■OH) and superoxide radicals (O_2■$^-$). Such highly reactive species are vital in breaking down organic dye molecules to non-toxic products.

In addition, the spinel Co_3O_4 structure consists of Co^{2+} ions in the tetrahedral sites and Co^{3+} ions in the octahedral sites, leading to efficient charge transfer dynamics. KOH-synthesized Co_3O_4 displayed a better uniform structure, which could result in better electron mobility and reduced charge recombination, while NH_4OH-synthesized Co_3O_4 had some less ordered structure that could lead to poor charge separation and lower photocatalytic activity

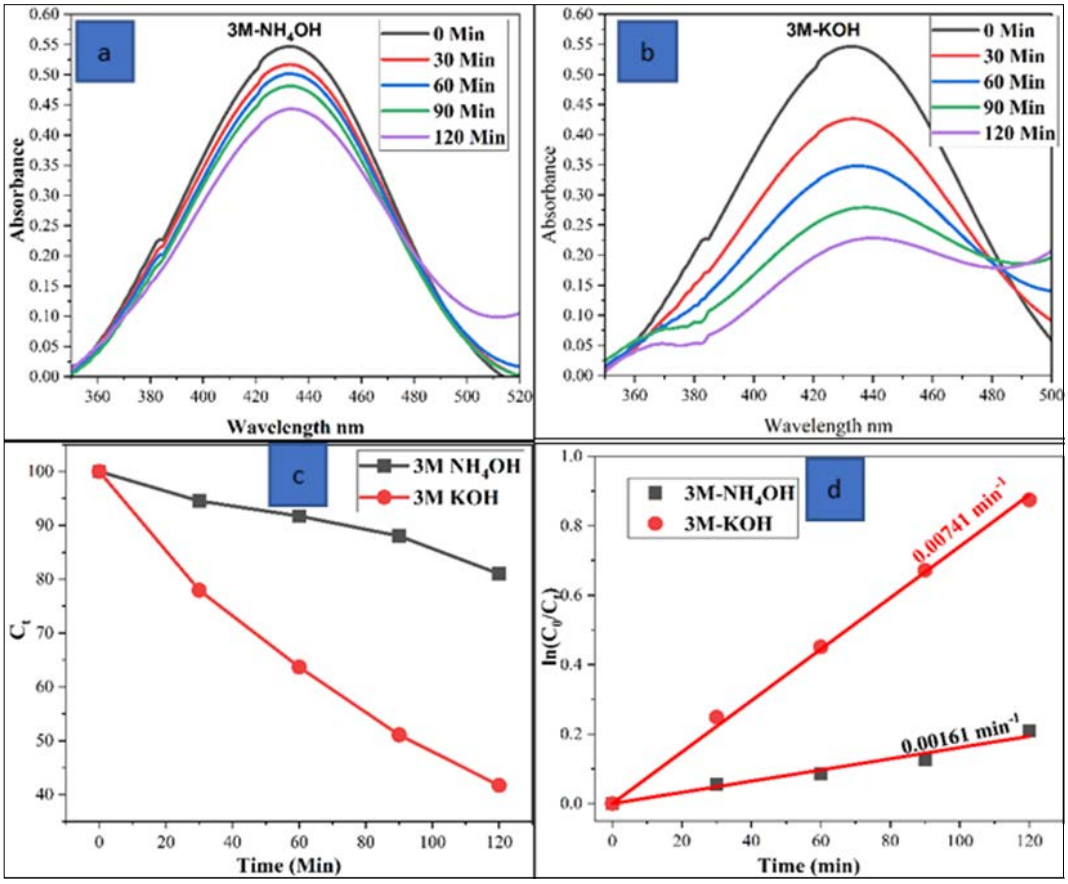

Fig 11: UV-Vis absorption spectra of phenol red dye in the presence of Co_3O_4 NPs synthesised with a) 3M-NH_4OH and b) 3M-KOH following sunlight irradiation. (c) Variation of PR concentration (%) with time (d) Rate kinetics of PR degradation

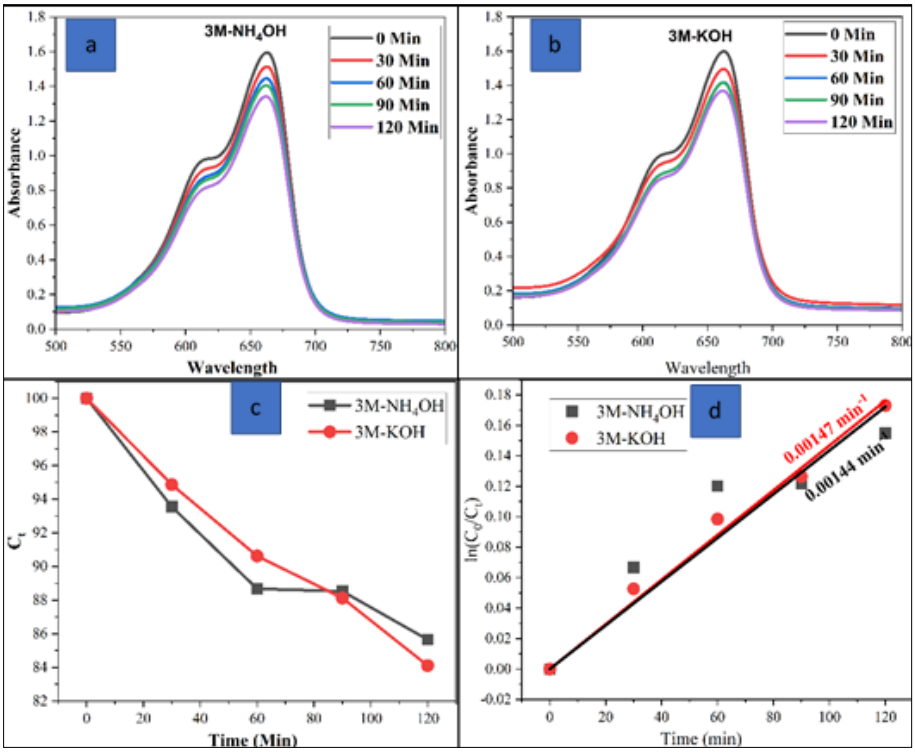

Fig 12: UV-Vis absorption spectra of Methylene Blue dye in the presence of Co_3O_4 NPs synthesised with a) 3M-NH_4OH and b) 3M-KOH following sunlight irradiation. (c) Variation of methylene blue concentration (%) with time (d) Rate kinetics of MB degradation

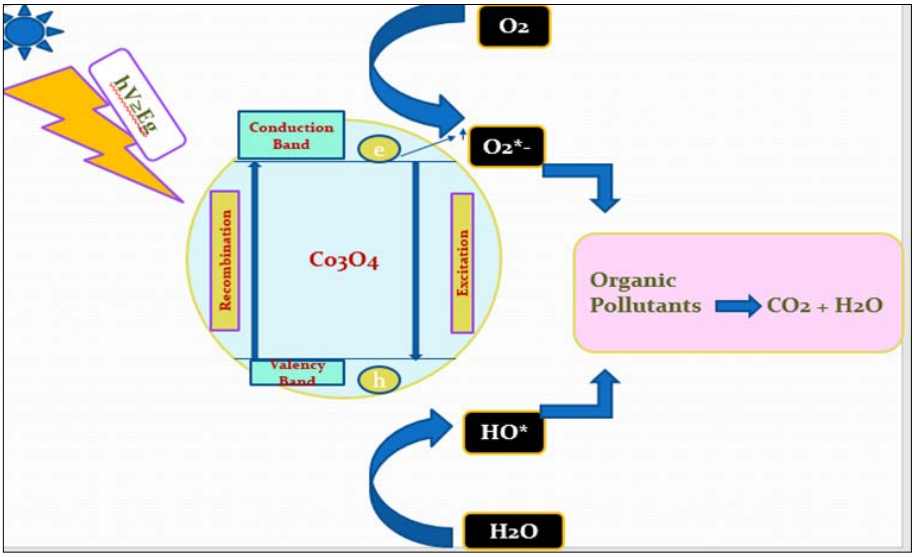

Fig 13: Diagrammatic representation of the photogenerated electron transit pathway during photocatalytic degradation in the Co_3O_4 nanostructure.

Clearly, Co_3O_4 is not an excellent photocatalyst for the degradation of MB. So, improvement of the activity of these particles is desired and can be obtained by improving Surface area to volume ratio, lowering band gap or lowering recombination rate of the electron-hole pairs generated (Fig.13). This can be done using the methods like metal doping, no metal doping, composite formation or functionalization to improve adsorption.

Conclusion

Co_3O_4-NPs were synthesised using an easy and facile co-precipitation method with potent oxidising capabilities. The synthesised NPs were examined using FTIR, XRD, FE-SEM, Raman, UV-vis, and other techniques; the outcomes showed that the synthesis of Co_3O_4-NPs was successful. The antibacterial activities of the synthesised Co_3O_4-NPs against both gram positive and gram-negative bacteria were investigated, yielding significant results. The maximum photocatalytic dye degradation was seen in Co_3O_4 nanoparticles synthesised with KOH as reducing agent due process. to their larger surface area and lower band energy. The results demonstrated that the KOH-synthesised Co_3O_4 nanoparticles had a moderate degree of photocatalytic activity and antibacterial effect. Co_3O_4 nanoparticles can be doped with additional suitable metal oxides to enhance their photocatalytic capabilities.

Furthermore, 3M-NH_4OH Co_3O_4 NPs were observed to exhibit lower percentage-wise dye degradation in the presence of sunshine. MB displayed significantly less breakdown activity than PR dye. It was discovered that

methylene blue only decreased at a rate of about 16% in 120 minutes, while phenol red dye degraded at a rate of almost 50%. Therefore, cobalt oxide nanoparticles synthesised in KOH can be used in the dye degradation

This study successfully synthesized Co_3O_4 nanoparticles using a simple co-precipitation method and evaluated their antimicrobial and photocatalytic properties. The characterization techniques confirmed the crystalline nature, purity, and morphology of the synthesized nanoparticles. Comparative analysis revealed that KOH-assisted Co_3O_4 nanoparticles exhibited superior antibacterial, antifungal, and photocatalytic performance compared to those synthesized with NH_4OH. The enhanced efficiency was attributed to their higher surface area, improved crystallinity, lower band gap, and better charge carrier separation, which facilitated greater dye degradation and microbial inhibition.

These findings contribute to the advancement of nanomaterial-based environmental and biomedical applications by demonstrating an optimized synthesis route for cobalt oxide nanoparticles with enhanced functional properties. The study highlights the potential of KOH-assisted Co_3O_4 synthesis as a scalable and cost-effective method for developing nanocatalysts with improved efficiency in wastewater treatment and antimicrobial applications. Furthermore, the results provide a foundation for future research on doping strategies, composite formation, and surface modifications to further enhance the photocatalytic and antibacterial properties of Co_3O_4-based material.

Acknowledgement

The authors are highly thankful to Dr.P.B.Undre, Department of Physics, Dr Babasaheb Ambedkar Marathwada University, Chhatrapati Sambhajinagar - 431004, India for providing the laboratory facilities. The authors wish special thanks to Abhijeet Pawar, Aakash Salmote and Mrs.Kahkashan Anjuman for rendering the helping hand in analysis part of the synthesised NPs.

References

1. Gour A, Jain NK. Advances in green synthesis of nanoparticles. Artificial Cells, Nanomedicine and Biotechnology,2019:47(1):844–851. doi: 10.1080/21691401.2019.1577878.
2. Azizi A. Green Synthesis of Fe3O4 Nanoparticles and Its Application in Preparation of Fe3O4/Cellulose Magnetic Nanocomposite: A Suitable Proposal for Drug Delivery Systems. J. Inorg. Organomet. Polym. Mater,2020:30(9):3552–3561. doi: 10.1007/s10904-020-01500-1.
3. Zeghoud S, *et al*. A review on biogenic green synthesis of ZnO nanoparticles by plant biomass and their applications. Mater. Today Commun,2022:33:104747. doi: 10.1016/j.mtcomm.2022.104747.
4. Umut E. Surface Modification of Nanoparticles Used in Biomedical Applications. in Modern Surface Engineering Treatments, InTech, 2013. doi: 10.5772/55746.
5. Chavali MS, Nikolova MP. Metal oxide nanoparticles and their applications in nanotechnology. SN Applied Sciences, 2019, 1(6). doi: 10.1007/s42452-019-0592-3.
6. Safdar A, Mohamed HEA, Hkiri K, Muhaymin A, Maaza M. Green Synthesis of Cobalt Oxide Nanoparticles Using *Hyphaene thebaica* Fruit Extract and Their Photocatalytic Application. Appl. Sci, 2023, 13(16). doi: 10.3390/app13169082.
7. Madhav S, Ahamad A, Singh P, Mishra PK. A review of textile industry: Wet processing, environmental impacts, and effluent treatment methods. Environ. Qual. Manag,2018:27(3):31–41. doi: 10.1002/tqem.21538.
8. Jesudoss SK, *et al*. High performance multifunctional green Co3O4 spinel nanoparticles: Photodegradation of textile dye effluents, catalytic hydrogenation of nitro-aromatics and antibacterial potential. Photochem. Photobiol. Sci,2017:16(5):766–778. doi: 10.1039/c7pp00006e.
9. Sha Y, *et al*. Rapid degradation of azo dye methyl orange using hollow cobalt nanoparticles. Chemosphere,2016:144:1530–1535. doi: 10.1016/j.chemosphere.2015.10.040.
10. "IJEAC.pdf."
11. Kumar S, Kaur G, Rawat M, Tsang YF, Lin KY, Kim KH. Potential of *Piper betle*@Co3O4 nanoparticles as high-performance photocatalysts for the removal of industrial dyes. J. Clean. Prod, 2022, 361. doi: 10.1016/j.jclepro.2022.132242.
12. Rasheed T, Nabeel F, Bilal M, Iqbal HMN. Biogenic synthesis and characterization of cobalt oxide nanoparticles for catalytic reduction of direct yellow-142 and methyl orange dyes. Biocatal. Agric. Biotechnol, 2019, 19. doi: 10.1016/j.bcab.2019.101154.
13. Saravan RS, *et al*. Evaluation of the photocatalytic efficiency of cobalt oxide nanoparticles towards the degradation of crystal violet and methylene violet dyes. Optik (Stuttg), 2020, 207. doi: 10.1016/j.ijleo.2020.164428.
14. Dou J, *et al*. Carbon spheres anchored Co3O4 nanoclusters as an efficient catalyst for dye degradation. Appl. Catal. A Gen,2016:513:106–115. doi: 10.1016/j.apcata.2015.12.028.
15. Sivachidambaram M, Vijaya JJ, Kaviyarasu K, Kennedy LJ, Al-Lohedan HA, Jothi Ramalingam R. A novel synthesis protocol for Co3O4 nanocatalysts and their catalytic applications. RSC Adv,2017:7(62):38861–38870. doi: 10.1039/c7ra06996k.
16. Chowdhury B, Pradhan SS, Das HS, Biswas B. Visible Light Induced Photocatalytic Dye Degradation by Cobalt Oxide Nanoparticles. Fine Chem. Eng, 2020, 104–117. doi: 10.37256/fce.122020559.
17. Ajarem JS, Maodaa SN, Allam AA, Taher MM, Khalaf M. Benign Synthesis of Cobalt Oxide Nanoparticles Containing Red Algae Extract: Antioxidant, Antimicrobial, Anticancer, and Anticoagulant Activity. J. Clust. Sci,2022:33(2):717–728. doi: 10.1007/s10876-021-02004-9.
18. Hassanpour M, Safardoust-Hojaghan H, Salavati-Niasari M. Degradation of methylene blue and Rhodamine B as water pollutants via green synthesized Co3O4/ZnO nanocomposite. J. Mol. Liq,2017:229:293–299. doi: 10.1016/j.molliq.2016.12.090.
19. Higgins MM, Toro González M, Rojas J. Enhanced X-RAYS degradation of methylene blue in the presence of gold microspheres. Radiat. Phys. Chem,2019:156:73–80. doi: 10.1016/j.radphyschem.2018.10.020.

20. Hiluf H, Yadav OP, Taddesse AM. Photo-Catalytic Degradation of Phenol Red Dye from Contaminated Water Over Nanosize Tio 2 , N-Doped-Tio 2 , Tio 2 /WO 3 and N-Doped Tio 2 /WO 3. Int J Pollut Res, 2019, 109. doi: 10.29011/IJPR.
21. Almulhem NK, Awada C. Study of Phenol Red Photocatalytic Decomposition on KBrO3-Supported TiO2 Study of Phenol Red Photocatalytic Decomposition on KBrO 3 -Supported TiO 2 Nanoparticles for Wastewater Treatment, 2023, (February). doi: 10.3390/separations10030162.
22. Moradpoor H, *et al*. Optimisation of cobalt oxide nanoparticles synthesis as bactericidal agents. Open Access Maced. J. Med. Sci,2019:7(17):2757–2762. doi: 10.3889/oamjms.2019.747.
23. Shete RC, *et al*. Issue 4 of Cobalt Oxide Nanoparticles: Green Synthesis, Biomedical Applications, and Toxicity Studies. J. Chem. Rev,2022:4(4):331–345. doi: 10.22034/JCR.2022.342398.1172.
24. Waris A, *et al*. Green fabrication of Co and Co3O4nanoparticles and their biomedical applications: A review. Open Life Sciences,2021:16(1):14–30. doi: 10.1515/biol-2021-0003.
25. Paul B, *et al*. Journal of Colloid and Interface Science Morphologically controlled cobalt oxide nanoparticles for efficient oxygen evolution reaction. J. Colloid Interface Sci,2021:582:322–332. doi: 10.1016/j.jcis.2020.08.029.
26. Haase FT, *et al*. reaction. 2022, 7(August). doi: 10.1038/s41560-022-01083-w.
27. Manoharadoss DD, Sadaiyandi PK. Precipitation method and characterization of cobalt oxide nanoparticles. Appl. Phys. A,2017:123(4):1–6. doi: 10.1007/s00339-017-0786-8.
28. Khalil A, Ali N, Khan A, Asiri AM, Kamal T. Catalytic potential of cobalt oxide and agar nanocomposite hydrogel for the chemical reduction of organic pollutants. Int. J. Biol. Macromol,2020:164:2922–2930. doi: 10.1016/j.ijbiomac.2020.08.140.
29. Chartier P, Poillerat G. Initial stages of cobalt oxidation by FTIR spectroscopy Initial stages of cobalt oxidation by FTIR spectroscopy, 2015, (December 1993). doi: 10.1051/jp4.
30. Danbature WL, Isyaka MS, Abdullahi MA, Gambo AA, Abdulmalik SS. UV-VIS, FTIR AND XRD CHARACTERIZATION OF SYNTHESIZED MAGNETIC COBALT (Co3O4) NANOPARTICLE USED IN CATALYTIC DECOMPOSITION OF HYDROGEN PEROXIDE. Fudma J. Sci,2024:7(6):222–227. doi: 10.33003/fjs-2023-0706-2105.
31. Structural and Optical Properties of Co 3 O 4 Nanoparticles Prepared by Sol-gel Technique for Photocatalytic Application,2019:14:3552. doi: 10.20964/2019.04.40.
32. Bukhamsin HA, Hammud HH, Awada C, Prakasam T. Catalytic Reductive Degradation of 4-Nitrophenol and Methyl orange by Novel Cobalt Oxide Nanocomposites. Catalysts,2024:14(1):89. doi: 10.3390/catal14010089.
33. Vennela AB, Mangalaraj D, Muthukumarasamy N, Agilan S, Hemalatha KV. Structural and optical properties of Co 3 O 4 nanoparticles prepared by sol-gel technique for photocatalytic application. Int. J. Electrochem. Sci,2019:14(4):3535–3552. doi: 10.20964/2019.04.40.
34. Raman V, *et al*. Synthesis of Co3O4 nanoparticles with block and sphere morphology, and investigation into the influence of morphology on biological toxicity. Exp. Ther. Med,2016:11(2):553–560. doi: 10.3892/etm.2015.2946.
35. Chelliah P, *et al*. Green Synthesis and Characterizations of Cobalt Oxide Nanoparticles and Their Coherent Photocatalytic and Antibacterial Investigations. Water (Switzerland), 2023, 15(5). doi: 10.3390/w15050910.
36. Saleh B, Fatema S, Farooqui M, Yusuf S. Cobalt Oxide Nanoparticles: Synthesis and Their Adsorption Study Article Info. J. Sci. Technol,2021:06(04):69–83. doi: 10.46243/jst.2021.v6.i4.pp69-83.
37. Sundararaju S, Arumugam M, Bhuyar P. *Microbacterium* sp . MRS-1 , a potential bacterium for cobalt reduction and synthesis of less / non-toxic cobalt oxide nanoparticles (Co 3 O 4), 2020.
38. Sabir FK, *et al*. Synthesis of Cobalt Oxide Nanoparticles Through Chemical and Biological Pathways for Antibacterial Activity Synthesis of Cobalt Oxide Nanoparticles Through Chemical and Biological Pathways for Antibacterial Activity, 2021, (February 2022). doi: 10.22052/JNS.2021.03.015.
39. Ghaedi M, Ansari A, Nejad PA, Ghaedi A, Vafaei A, Habibi MH. Artificial neural network and bees algorithm for removal of eosin b using cobalt oxide nanoparticle-activated carbon: Isotherm and kinetics study. Environ. Prog. Sustain. Energy,2015:34(1):155–168. doi: 10.1002/ep.11981.
40. Khusnuriyalova AF, Caporali M, Hey-hawkins E, Sinyashin OG. Preparation of Cobalt Nanoparticles, 2021, 3023–3047. doi: 10.1002/ejic.202100367.
41. Letsholathebe D, *et al*. Optical and structural stability of Co3O4nanoparticles for photocatalytic applications. in Materials Today: Proceedings, Elsevier Ltd, 2019, 499–503. doi: 10.1016/j.matpr.2020.05.205.
42. Alwin David S, Doss A, Powel Praveen Pole R, Pushpabai Kumari Pushpa Rani T, Padma Latha Reshmi R, Rajalakshmi R. Synthesis and characterization of Cobalt Oxide nanoparticles using *Momordica charantia* and its photocatalytic activity, 2022.
43. Samuel MS, *et al*. Green synthesis of cobalt-oxide nanoparticle using jumbo Muscadine (*Vitis rotundifolia*): Characterization and photo-catalytic activity of acid Blue-74. J. Photochem. Photobiol. B Biol, 2020. doi: 10.1016/j.jphotobiol.2020.112011.
44. Hafeez M, *et al*. Green synthesis of cobalt oxide nanoparticles for potential biological applications. Mater. Res. Express, 2020, 7(2). doi: 10.1088/2053-1591/ab70dd.
45. Omran BA, *et al*. Novel mycosynthesis of cobalt oxide nanoparticles using *Aspergillus brasiliensis* ATCC 16404—optimization, characterization and antimicrobial activity. J. Appl. Microbiol,2020:128(2):438–457. doi: 10.1111/jam.14498.
46. Adekunle AS, *et al*. Potential of cobalt and cobalt oxide nanoparticles as nanocatalyst towards dyes degradation in wastewater, vol. 21. Elsevier B.V, 2020. doi: 10.1016/j.nanoso.2019.100405.